Free-surface instability in electro-osmotic flows of ultrathin liquid films

Manik Mayur, Sakir Amiroudine, Didier Lasseux

PHYSICAL REVIEW E, 2012, **85**, 046301 (12pp), DOI: 10.1103/PhysRevE.85.046301

Free-surface instability in electro-osmotic flows of ultrathin liquid films

Manik Mayur and Sakir Amiroudine
Université Bordeaux 1, Institut de Mécanique et d'Ingénierie - TREFLE, UMR CNRS 5295, 16 avenue Pey-Berland, F-33607 Pessac Cedex, France

Didier Lasseux
Institut de Mécanique et d'Ingénierie - TREFLE, UMR CNRS 5295, Esplanade des Arts et Métiers, F-33400 Talence Cedex, France

(Received 6 September 2011; published 3 April 2012)

The stability of a free surface under electro-osmotic flow in thin liquid films is investigated where the film thickness can be varied over the scale of a thick to thin electrical double layer while considering the relative contribution from the van der Waals forces. The role of interfacial Maxwell stress on thin film stability is highlighted. This configuration gives some interesting insights into the physics of free surface stability at a scale where various competing forces such as the Coulombic force, van der Waals force, and surface tension come into play. The effects of the mentioned forces are incorporated in the Navier-Stokes equations and a linear stability analysis of the resulting governing equations is performed to obtain the Orr-Sommerfeld equations. The characteristic stability curve of the system is obtained through an asymptotic analysis of the Orr-Sommerfeld equations in the long wave limit. In this study, special focus is given to the effect of the interfacial zeta potential on the free surface stability. It is found that when the free surface and the substrate zeta potential have the same polarity the system is unstable. Since the strength of the free surface potential depends upon the nature of the fluid substrate interaction, this study can help in choosing a proper combination of fluid and substrate to design microfluidic and nanofluidic channels with a desired flow rate without triggering the interfacial instability.

I. INTRODUCTION

Stability of fluid interfaces under electro-osmotic flow has been a wide field of research in the past decade [1–6]. A variety of stability models have been presented, discussing the effects of flow-actuating parameters, along with substantial experimental evidence to validate the theoretical predictions [7–10]. However, most of the mentioned studies have been concentrated in the domain where the electrical double layer (EDL) is negligible as compared to the characteristic length scale. In such domains, the effect of the EDL on the flow is modeled using a slip velocity, which is obtained by the classical Helmholtz-Smoluchoski formulation [11]. This approximation has been substantially helpful to design the flow and mixing process in modern microfluidic devices. However, with the technology of miniaturization foraying in the nanometric length scale with some applications like the controlled delivery of nonconducting liquids in microfluidics devices, patterned conformal coatings, and control of thin films on electrostatic film radiators in space applications [12], the fluid dynamics within the limits of the EDL cannot be ignored. It has been established that new modes of instability can be observed when the Debye length is comparable to the film thickness [13]. In some of earlier works [13–16], the effects of electric field strength, surface tension, and intermolecular van der Waals force on free surface instability, where the length scale is of the order of the Debye length, have been discussed. However, the effect of electric-field-generated stress (Maxwell stress) at the free surface has been overlooked. This Maxwell stress at the free surface is engendered due to the presence of free charges, the magnitude of which depends upon the fluid properties and substrate fluid interactions. It has been recently shown that due to the Maxwell stress, the free surface has an active role in electro-osmotic flows and should not be treated as a passive entity [16]. The motivation behind this study is to provide a collective insight in the free surface stability of thin films where the EDL is participating actively in the flow driving mechanism. In this work, the role of individual physical parameters like surface tension, disjoining pressure, applied electric field, substrate zeta potential, free surface potential, film thickness, and Debye length on the thin film stability is identified. The linear stability analysis of the governing equations is performed to obtain Orr-Sommerfeld equations. These equations are solved by the asymptotic long wave expansion method of Yih [17]; as for thin viscous films, the instability is found to occur at long wavelengths [18]. This paper is divided in three sections. In the first section, the characteristics of the physical system under investigation is presented. The contributions of various parameters to the governing equations are also worked out. In the second section, linear stability analysis of the system is performed and the characteristic stability curve is obtained as a solution of the Orr-Sommerfeld equations. Finally, an extensive discussion on the parametric dependence of the stability of the system is presented.

II. PHYSICAL SYSTEM

The physical system under study consists of a thin film of ionic solution that develops an EDL upon getting in contact with a solid substrate (see Fig. 1). The free surface of the thin film is exposed to a static inert atmosphere which remains

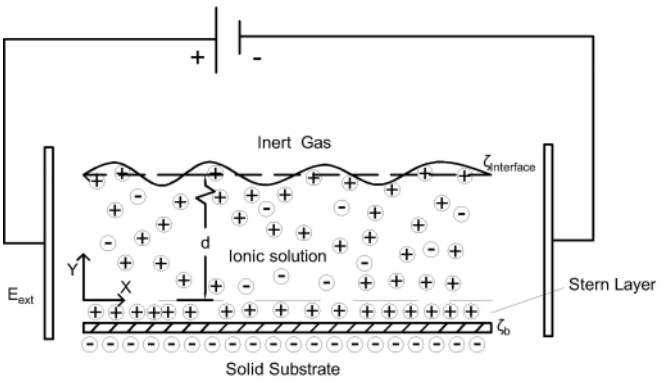

FIG. 1. Schematic of the two-dimensional thin film system.

at a constant pressure. The zeta potential of the substrate is represented by ζ_b. Due to the specific ion adsorption [19] at the liquid-gas interface, the resulting zeta potential is represented by $\zeta_{\text{Interface}}$. The magnitude of the external electric field is taken as E_{ext} and the initial film thickness is taken as d while the location of the free surface is represented by $y = h(x,t)$.

The fluid considered here is taken to be an aqueous solution of a symmetric electrolyte with low concentration to neglect the Joule heating effects [20]. This ensures constant fluid properties, even upon the application of large electric fields. Working with such a low concentration generates also the Debye length of the order of the thickness of the fluid film considered in this study. The low concentration study allows us to use the Debye-Huckel formulation for a potential field in an electric double layer with an assumption that the external electric field has no effect on the ionic distribution in the double layer. Hence, the net electrical potential field in the system is developed as a superposition of two potential fields. The first one is due to the formation of the EDL and is represented by the potential $\phi_1(y)$. The second field is due to the external electric field E_{ext}, which is represented as a gradient of the potential $\phi_2(x)$. Hence, the net electric potential in the system can be written as $\phi(x,y) = \phi_1(y) + \phi_2(x)$. Upon using the classical Poisson-Boltzmann formulation the EDL potential distribution is obtained as

$$\frac{d^2\phi_1}{dy^2} = -\frac{\rho_e}{\epsilon}, \tag{1}$$

where ρ_e is the charge density and ϵ is the dielectric permittivity of the ionic solution. The net charge density follows the Boltzmann distribution and can be written as

$$\rho_e = -2ze\rho_0 \text{Sinh}\left(\frac{ez\phi_1}{k_B\theta}\right), \tag{2}$$

where ρ_0, z, k_B, θ, and e are, respectively, the bulk ionic density, the valence of the ions in the aqueous phase, the Boltzmann constant, the temperature, and the electronic charge. The electric potential distribution upon substituting the value of charge distribution from Eq. (2) can be written as

$$\frac{d^2\phi_1}{dy^2} = \frac{2ze\rho_0}{\epsilon}\text{Sinh}\left(\frac{ez\phi_1}{k_B\theta}\right). \tag{3}$$

The electrical potential field $\phi_2(x)$ due to the external electric field E_{ext} can be expressed as

$$E_{\text{ext}} = -\frac{d\phi_2}{dx}. \tag{4}$$

Upon using nondimensional parameters as $\Phi_1 = \phi_1/\zeta_b$, $\Phi_2 = \phi_2/\zeta_b$, $X = x/d$, $Y = y/d$, $H = h/d$, Eq. (3) can be written as

$$\frac{d^2\Phi_1}{dY^2} = \beta\text{Sinh}(\chi\Phi_1), \tag{5}$$

where $\beta = (kd)^2/\chi$, $\chi = (ez\zeta_b)/(k_B\theta)$ is the ionic energy parameter and k is the Debye-Huckel parameter, which is defined as the inverse of the Debye length $\lambda_D = \sqrt{(\epsilon k_B\theta)/(2\rho_0 z^2e^2)}$. Within the approximation of Debye Huckel linearization, which is valid for $\chi \ll 1$, the resulting linearized Poisson Boltzmann equation can be written as

$$\frac{d^2\Phi_1}{dY^2} = \beta\chi\Phi_1. \tag{6}$$

The associated boundary conditions on the potential are given by $\Phi_1(0) = 1, \Phi_1(H) = Z_R$, where $Z_R = \zeta_{\text{Interface}}/\zeta_b$ is the ratio of the zeta potential at the free surface and at the substrate. The zeta potential at the free surface is a function of a variety of parameters involving fluid and substrate properties and can be measured using various specifically designed instruments [21]. Upon solving Eq. (6) with the mentioned boundary conditions, the electrostatic potential distribution $\Phi_1(Y)$ can be obtained as

$$\Phi_1(Y) = \frac{1}{\text{Sinh}\left(\frac{H}{N_D}\right)}\left\{Z_R\text{Sinh}\left(\frac{Y}{N_D}\right) + \text{Sinh}\left(\frac{H-Y}{N_D}\right)\right\}, \tag{7}$$

where $N_D = \lambda_D/d = 1/\sqrt{\chi\beta}$ is the Debye number.

Upon using the dimensionless variables, the external electric-field-generated potential, $\Phi_2(X)$ obeys the following relationship:

$$\frac{d\Phi_2}{dX} = -\frac{E_{\text{ext}}d}{\zeta_b} = -\frac{1}{E_R}, \tag{8}$$

where $E_R = \zeta_b/(E_{\text{ext}}d)$ is the relative strength of the zeta potential to the applied electric field. Hence the solution for $\Phi_2(X)$ with the boundary condition $\Phi_2(0) = 0$ can be obtained as

$$\Phi_2(X) = -\frac{X}{E_R}. \tag{9}$$

Hence, the total electric potential can be written as

$$\Phi(X,Y) = \Phi_1(Y) + \Phi_2(X) = -\frac{X}{E_R} + \frac{1}{\text{Sinh}\left(\frac{H}{N_D}\right)} \times \left\{Z_R\text{Sinh}\left(\frac{Y}{N_D}\right) + \text{Sinh}\left(\frac{H-Y}{N_D}\right)\right\}. \tag{10}$$

The corresponding electric field can be calculated as $\mathbf{E} = -\nabla\phi$.

The external electric field also leads to Maxwell stress ($\boldsymbol{\Sigma}^M$) on the fluidic system. Thus the total stress ($\boldsymbol{\Sigma}^T$) acting on the

fluid can be written as a combination of both hydrodynamic ($\boldsymbol{\Sigma}^{\boldsymbol{H}}$) and Maxwell stress components as

$$\begin{aligned}\boldsymbol{\Sigma}^{\boldsymbol{T}} &= \boldsymbol{\Sigma}^{\boldsymbol{H}} + \boldsymbol{\Sigma}^{\boldsymbol{M}} \\ &= -\left(p + \frac{\varepsilon|\boldsymbol{E}|^2}{2}\right)\boldsymbol{I} + \mu(\boldsymbol{\nabla u} + \boldsymbol{\nabla u}^T) + \varepsilon \boldsymbol{E}\boldsymbol{E}, \quad (11)\end{aligned}$$

where the Maxwell stress tensor $\boldsymbol{\Sigma}^{\boldsymbol{M}}$ in the absence of magnetic field can be written as

$$\boldsymbol{\Sigma}^{\boldsymbol{M}} = -\frac{\varepsilon|\boldsymbol{E}|^2}{2}\boldsymbol{I} + \varepsilon \boldsymbol{E}\boldsymbol{E}. \quad (12)$$

In problems involving thin films where the Debye length is of the order of the film thickness, the effect of intermolecular interactions cannot be ignored. This intermolecular interaction manifests itself in the form of a disjoining pressure term in momentum equations. The disjoining pressure as defined by Derjaguin *et al*. [22] corresponds to the excess pressure needed to maintain mechanical equilibrium between the pressure buildup in the liquid film due to the thinning process and the pressure applied to the surface of the film. It is represented as a pressure term in the momentum equations and its dominant molecular component is defined as

$$p_d = -\frac{a}{6\pi h^3}, \quad (13)$$

where a is the Hamaker's constant and h is the film thickness.

III. GOVERNING EQUATIONS

The mass and momentum conservation equations for a Newtonian fluid with incompressible flow can be written as

$$\begin{aligned}\boldsymbol{\nabla}\cdot\boldsymbol{u} &= 0, \\ \rho\left[\frac{\partial \boldsymbol{u}}{\partial t} + (\boldsymbol{u}\cdot\boldsymbol{\nabla})\boldsymbol{u}\right] &= -\boldsymbol{\nabla}(p + p_d) + \mu\nabla^2\boldsymbol{u} + \boldsymbol{\nabla}\cdot\boldsymbol{\Sigma}^{\boldsymbol{M}} \\ &= -\boldsymbol{\nabla} p_d + \boldsymbol{\nabla}\cdot\boldsymbol{\Sigma}^{\boldsymbol{T}}. \quad (14)\end{aligned}$$

At the substrate, no-slip and no-penetration conditions are assumed. At the free surface, which is located at $y = h(x,t)$, the jump of shear and normal stresses can be written as, respectively,

$$[\boldsymbol{t}\cdot\boldsymbol{\Sigma}^{\boldsymbol{T}}\cdot\boldsymbol{n}] = 0, \quad (15)$$

$$[\boldsymbol{n}\cdot\boldsymbol{\Sigma}^{\boldsymbol{T}}\cdot\boldsymbol{n}] = \gamma\kappa, \quad (16)$$

where $\gamma\kappa$ is the capillary force with γ being the surface tension and κ the local curvature of the interface. The dimensionless equations are written using the viscous time scale $T = t\nu/d^2$. The corresponding dimensionless velocities and pressure are then $U = u\,d/\nu$, $V = v\,d/\nu$, and $P = p\,d^2/(\rho\nu^2)$. These equations can hence be written as

$$\frac{\partial U}{\partial X} + \frac{\partial V}{\partial Y} = 0, \quad (17)$$

$$\begin{aligned}\frac{\partial U}{\partial T} + U\frac{\partial U}{\partial X} + V\frac{\partial U}{\partial Y} &= -\frac{\partial P}{\partial X} + \frac{3AH_x}{H^4} + \frac{\partial^2 U}{\partial X^2} + \frac{\partial^2 U}{\partial Y^2} \\ &\quad + N_{EO}E_R\frac{\partial\Phi}{\partial X}\left(\frac{\partial^2\Phi}{\partial X^2} + \frac{\partial^2\Phi}{\partial Y^2}\right), \quad (18)\end{aligned}$$

$$\begin{aligned}\frac{\partial V}{\partial T} + U\frac{\partial V}{\partial X} + V\frac{\partial V}{\partial Y} &= -\frac{\partial P}{\partial Y} + \frac{\partial^2 V}{\partial X^2} + \frac{\partial^2 V}{\partial Y^2} \\ &\quad + N_{EO}E_R\frac{\partial\Phi}{\partial Y}\left(\frac{\partial^2\Phi}{\partial X^2} + \frac{\partial^2\Phi}{\partial Y^2}\right), \quad (19)\end{aligned}$$

where $N_{EO} = (\varepsilon E_{\text{ext}} d\zeta_b)/(\rho\nu^2)$ is the electro-osmotic number, $A = -a/(6\pi\rho d\nu^2)$ is a dimensionless disjoining pressure parameter. The dimensionless boundary conditions at the substrate ($Y = 0$) are

$$U(X,0) = 0, \quad V(X,0) = 0. \quad (20)$$

The continuity of shear and normal stresses at the free surface $Y = H(X,T)$ can be written as, respectively,

$$\left[\left(\frac{\partial U}{\partial Y} + \frac{\partial V}{\partial X}\right)\left\{1 - \left(\frac{\partial H}{\partial X}\right)^2\right\} - 4\frac{\partial H}{\partial X}\frac{\partial U}{\partial X}\right] + N_{EO}E_R\left[\frac{\partial\Phi}{\partial X}\frac{\partial\Phi}{\partial Y}\left\{1 - \left(\frac{\partial H}{\partial X}\right)^2\right\} - \frac{\partial H}{\partial X}\left\{\left(\frac{\partial\Phi}{\partial X}\right)^2 - \left(\frac{\partial\Phi}{\partial Y}\right)^2\right\}\right] = 0, \quad (21)$$

$$\begin{aligned}&-\left[P + \frac{N_{Eo}E_R}{2}\left\{\left(\frac{\partial\Phi}{\partial X}\right)^2 + \left(\frac{\partial\Phi}{\partial Y}\right)^2\right\}\right] + \frac{2}{\left\{1 + \left(\frac{\partial H}{\partial X}\right)^2\right\}}\left[\frac{\partial U}{\partial X}\left\{\left(\frac{\partial H}{\partial X}\right)^2 - 1\right\} - \frac{\partial H}{\partial X}\left(\frac{\partial U}{\partial Y} + \frac{\partial V}{\partial X}\right)\right] \\ &+ \frac{N_{EO}E_R}{\left\{1 + \left(\frac{\partial H}{\partial X}\right)^2\right\}}\left\{\left(\frac{\partial\Phi}{\partial X}\right)^2\left(\frac{\partial H}{\partial X}\right)^2 + \left(\frac{\partial\Phi}{\partial Y}\right)^2 - 2\frac{\partial H}{\partial X}\frac{\partial\Phi}{\partial X}\frac{\partial\Phi}{\partial Y}\right\} = \frac{S\frac{\partial^2 H}{\partial X^2}}{\left\{1 + \left(\frac{\partial H}{\partial X}\right)^2\right\}^{\frac{3}{2}}}, \quad (22)\end{aligned}$$

where $S = \gamma d/\rho\nu^2$ is the dimensionless surface tension parameter.

The kinematic condition at the free surface $Y = H(X,T)$ is the following:

$$V = \frac{\partial H}{\partial T} + U\frac{\partial H}{\partial X}. \quad (23)$$

IV. LINEAR STABILITY ANALYSIS

A. Basic state solution

The basic state solution is obtained by considering the film to be of uniform thickness. The problem hence reduces to a one-dimensional steady flow (velocity $U_b(Y)$) with a flat interface ($H(X,T) = 1$). The base state governing equations in dimensionless form are

$$\partial U_b/\partial X = 0, \tag{24}$$

$$0 = \frac{\partial^2 U_b}{\partial Y^2} + \frac{N_{EO}}{N_D^2 \mathrm{Sinh}\left(\frac{1}{N_D}\right)} \times \left\{ Z_R \mathrm{Sinh}\left(\frac{Y}{N_D}\right) + \mathrm{Sinh}\left(\frac{1-Y}{N_D}\right) \right\}. \tag{25}$$

The no-slip condition at the substrate ($Y = 0$) leads to

$$U_b(0) = 0, \tag{26}$$

and the continuity of shear and normal stresses at $Y = 1$ are respectively

$$\frac{dU_b}{dY} + N_{EO} E_R \frac{\partial \Phi}{\partial X}\frac{\partial \Phi}{\partial Y} = 0, \tag{27}$$

$$-P_b - \frac{N_{EO} E_R}{2}\left\{ \left(\frac{\partial \Phi}{\partial X}\right)^2 + \left(\frac{\partial \Phi}{\partial Y}\right)^2 \right\} + N_{EO} E_R \left(\frac{\partial \Phi}{\partial Y}\right)^2 = 0. \tag{28}$$

From Eqs. (24) to (28), the solution for $U_b(Y)$ can be obtained as follows:

$$U_b(Y) = -N_{EO}\left(1 - \frac{Z_R \mathrm{Sinh}\left(\frac{Y}{N_D}\right) + \mathrm{Sinh}\left(\frac{1-Y}{N_D}\right)}{\mathrm{Sinh}\left(\frac{1}{N_D}\right)}\right). \tag{29}$$

The fluid velocity at the free surface is then

$$U_b(1) = N_{EO}(Z_R - 1), \tag{30}$$

which has a linear dependence upon the zeta potential at the interface. This dependence can facilitate or delay the free surface stability by either increasing or decreasing the shear stress [16].

B. Normal mode analysis

The perturbation in flow variables is introduced as follows:

$$\begin{aligned} U(X,Y,T) &= U_b(Y) + \tilde{U}(X,Y,T), \\ V(X,Y,T) &= \tilde{V}(X,Y,T), \\ P(X,Y,T) &= P_b(Y) + \tilde{P}(X,Y,T), \\ H(X,T) &= 1 + \tilde{H}(X,T), \end{aligned} \tag{31}$$

where variables with a tilde correspond to perturbation variables. To reduce the number of dependent variables, the stream function is introduced as $\tilde{U} = \frac{\partial \tilde{\Psi}}{\partial Y}, \tilde{V} = -\frac{\partial \tilde{\Psi}}{\partial X}$. Using the normal mode analysis with perturbation parameters given as $\tilde{\Psi}(X,Y,T) = \Psi(Y)e^{i\alpha(X-CT)}, \tilde{P}(X,Y,T) = \Pi(Y)e^{i\alpha(X-CT)}, \tilde{H}(X,T) = \eta e^{i\alpha(X-CT)}$, where α is the wave number and C is the wave velocity, the Orr-Sommerfeld equations are obtained by eliminating pressure terms from the governing set of equations. The resulting eigenvalue problem is given by

$$\begin{aligned} &(D^2-\alpha^2)^2\Psi(Y) + i\alpha\left[(C-U_b)(D^2-\alpha^2) + \frac{d^2U_b}{dY^2}\right]\Psi(Y) = 0, \quad \Psi(0) = D\Psi(0) = 0, \\ &(D^2-3\alpha^2)\Psi(1) + i\alpha\left[\Psi(1)\frac{dU_b(1)}{dY} + [C-U_b(1)]D\Psi(1)\right] + i\alpha\eta(3A-\alpha^2 S) = 0, \\ &(D^2+\alpha^2)\Psi(1) + \frac{d^2U_b}{dY^2} - i\alpha\eta N_{EO}E_R\left[\left(\frac{\partial\Phi}{\partial X}\right)^2 - \left(\frac{\partial\Phi}{\partial Y}\right)^2\right] = 0, \quad \Psi(1) + \eta[C-U_b(1)] = 0, \end{aligned} \tag{32}$$

where $D = \frac{d}{dY}$.

In thin film stability problems, the long wave analysis of the resulting Orr-Sommerfeld equations yields results that capture the essential features of the full numerical solution of the complex set of equations. Hence the stability information of thin film systems can be recovered without solving the complete set of equations. Here, Yih's method [17] is used to expand the dependent variables like Ψ and C in powers of α and solve equations at zeroth and first orders in α with the assumption that $\alpha^2 S \sim O(1)$, which is valid for thin film flows [23]. As a consequence we use the developments

$$\begin{aligned} \Psi &= \Psi_0 + i\alpha\Psi_1 - \alpha^2\Psi_2, \ldots, \\ C &= C_0 + i\alpha C_1 - \alpha^2 C_2, \ldots. \end{aligned} \tag{33}$$

Upon substituting the expansion of the wave velocity Eq. (33)] in the perturbation term $\tilde{\Psi}(X,Y,T)$ and ignoring the higher powers of $\alpha[\sim O(\alpha^3)]$, we obtain

$$\tilde{\Psi}(X,Y,T) = \Psi(Y)e^{\alpha^2 C_1 T}e^{i\alpha(X-C_0T)}. \tag{34}$$

It can be seen that the marginal stability curves for the system can be obtained with $\alpha^2 C_1 = 0$, which in turn provides the marginal stability characteristic equation for the system. The solution for C_1 is worked out in the Appendix. Here $\alpha^2 C_1$ is equivalent to the real part of the growth rate (σ_R) in classical formulation. The characteristic stability curves are graphically presented by plotting the variation of σ_R versus α in the range of $\alpha \leqslant O(1)$ (i.e., in the long wave limit).

The flow actuating mechanism in this study is the externally applied electric field, which acts as a body force in the fluid bulk and manifests itself as the Maxwell stress on the free surface. Its contribution is reflected in the two dimensionless numbers, namely, N_{EO} and E_R. It has to be noted that, by definition, the mentioned dimensionless numbers also depend upon another imposed field variable: the substrate zeta potential. To study the effect of the imposed electric field and the substrate zeta potential separately, the following combination of N_{EO} and E_R is presented. By varying the ratio $(\frac{N_{EO}}{E_R})$ one can study the effect of the variation of the electric field on the stability of the system. While selectively varying the product $(N_{EO}E_R)$ one can study the effect of the variation of the substrate zeta potential on the stability of the system. The other important parameters which have a significant effect on free surface stability are the dimensionless Hamaker constant (A), the Debye number (N_D), the surface tension parameter (S), and the ratio of the interfacial to substrate zeta potential (Z_R). The real part of the growth rate, σ_R as obtained from the solution of the Orr-Sommerfeld equations from asymptotic analysis, can be written as

$$\sigma_R = f(S)\alpha^4 + g(A, N_{EO}, E_R, Z_R, N_D)\alpha^2, \tag{35}$$

where

$$f(S) = -\frac{S}{3}, \tag{36}$$

and

$$\begin{aligned} g(A, N_{EO}, E_R, Z_R, N_D) = A + \frac{N_{EO}}{2E_R} - \left\{\text{Cosech}\left(\frac{1}{N_D}\right) - Z_R\text{Coth}\left(\frac{1}{N_D}\right)\right\}^2 N_{EO}E_R \\ - \left\{9N_D^2 - 5N_D\text{Coth}\left(\frac{1}{N_D}\right) + \left(\frac{1}{N_D} - 4N_D\right)\text{Cosech}\left(\frac{1}{N_D}\right)\right\} N_{EO}^2 Z_R \\ + \left\{\frac{5}{48N_D^4} - \frac{11}{24N_D^2} - \frac{1}{2} + 9N_D^2 + \left(\frac{1}{N_D} - 4N_D\right)\text{Coth}\left(\frac{1}{N_D}\right) - 5N_D\text{Cosech}\left(\frac{1}{N_D}\right)\right\} N_{EO}^2 Z_R^2. \end{aligned} \tag{37}$$

V. RESULTS AND DISCUSSION

To highlight the role of the interfacial Maxwell stress on the thin film stability, two characteristic stability curves were worked out. The first was obtained by removing the Maxwell stress term $\mathbf{\Sigma}_M$ from the total stress term $\mathbf{\Sigma}_T$ in the free surface boundary conditions. This method brings out the analysis in which the electric field contributes as a body force only in the momentum equations. The second characteristic stability curve was obtained by keeping the Maxwell stress term in the total stress at the free surface boundary condition. Upon plotting the real part of the growth rate against the wave number for both cases, it was found that ignoring the Maxwell stress on the free surface overestimates the instability (see Fig. 2). This overprediction can significantly affect the sensitive dependence of the stability of the system which is a function of a large number of the mentioned parameters. The parametric dependence of the stability of the system will be discussed henceforth within the purview of the model that includes the contribution of the Maxwell stress at the free surface.

The order of magnitude analysis on Eq. (18), highlights the relative contribution of the two important phenomena, namely, disjoining pressure and Maxwell stress to the thin

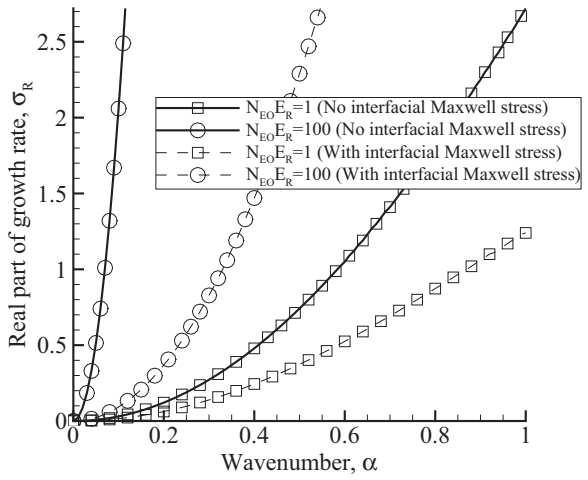

FIG. 2. Comparison of the variation of the real part of growth rate (σ_R) as a function of the wave number (α) for $S = 1, Z_R = 1$, $N_D = 0.5, A = 1$.

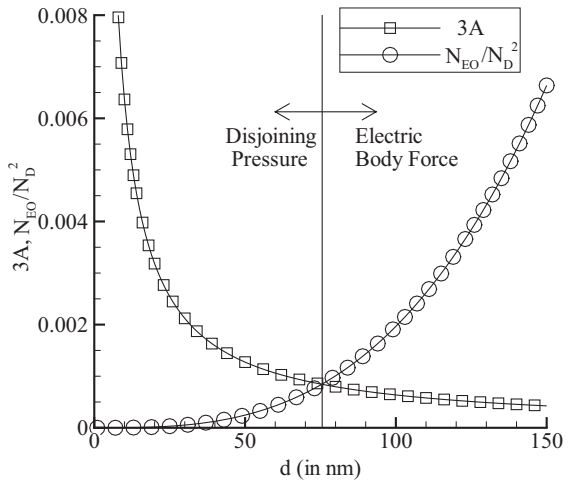

FIG. 3. Comparison of the dimensionless contributions of disjoining pressure $3A$ and Maxwell stress as a function of the film thickness d keeping the values of other parameters fixed.

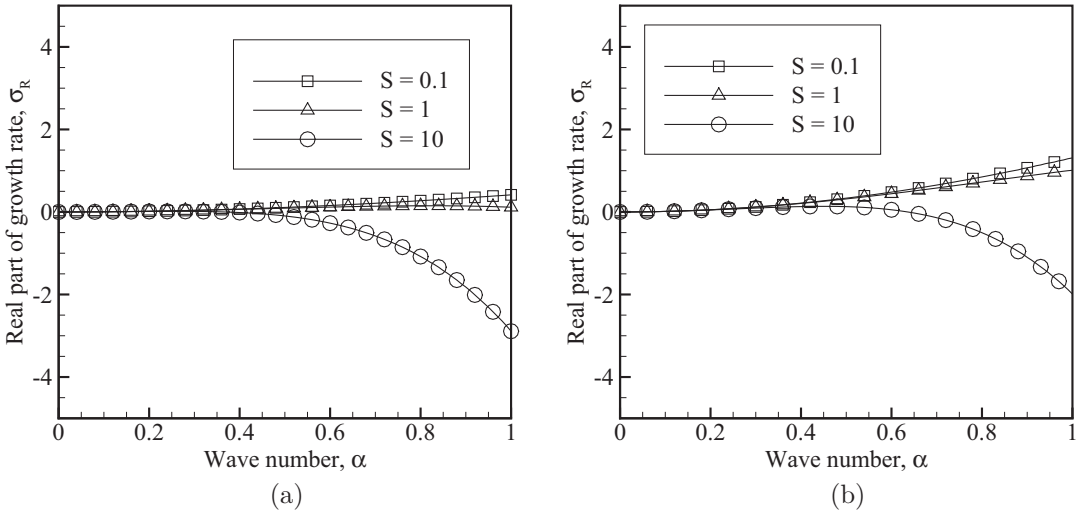

FIG. 4. Growth rate variation with the wave number for different values of the dimensionless surface tension parameter S with $N_{EO}E_R = 1$, $N_D = 0.5$, $Z_R = 0$ and (a) $A = 0.1$, (b) $A = 1$.

film dynamics. Using Eq. (10), one can show that the Maxwell stress contribution to the momentum equation represented by $N_{EO}E_R\frac{\partial\Phi}{\partial X}\nabla^2\Phi$ term reduces to the order $\sim O(\frac{N_{EO}}{(N_D)^2})$. The variation of $\frac{N_{EO}}{N_D^2}$ and $3A$ (representing the disjoining pressure) can be plotted (see Fig. 3) as a function of d for fixed values of the parameters for a typical water-air system: $\rho \sim 10^3$ kg/m^3, $\gamma \sim 0.1$ N/m, $a \sim -10^{-19}$ J, $\nu \sim 10^{-6}$ m^2/s, $\epsilon \sim 80\,\epsilon_0$ F/m where ϵ_0 is the permittivity of vacuum. The typical values of controllable parameters are taken as $\zeta_b = 25$ mV, $E_{\text{ext}} = 10^6$ V/m, $c_0 = 0.01$ mM. In Fig. 3 the two curves $3A$ and N_{EO}/N_D^2 versus d are giving an intersection point which demarcates two zones showing the relative dominance of the two novel effects, disjoining pressure and Maxwell stress. In the above case the value of the corresponding film thickness is approximately 76 nm. So this means that for the given values of parameters if film thickness is greater than 76 nm, the effect of disjoining pressure will be less compared to the Maxwell stress.

Figure 4 shows the growth rate σ_R as a function of the wave number for different values of the surface tension parameter S and two values of the Hamaker's constant A. All the other parameters are taken as fixed. For both values of A, the system becomes more stable at large values of the wave number as the surface tension parameter S increases. This can also be observed from Eqs. (35) and (36). While at the small wave numbers, that is, in the domain of long wave disturbances, the stabilizing effect of surface tension diminishes.

It can also be seen that the disjoining pressure represented through the dimensionless constant A has a significant effect on the stability of the system in the long wave domain. Figure 5 shows the effect of A on the growth rate, σ_R for fixed values of electrical field E_{ext} [Fig. 5(a)], and substrate zeta potential ζ_b [Fig. 5(b)]. From these figures it is observed that upon increasing the disjoining pressure, the system becomes unstable. This phenomenon can be explained by the fact that increasing the disjoining pressure pushes the system away

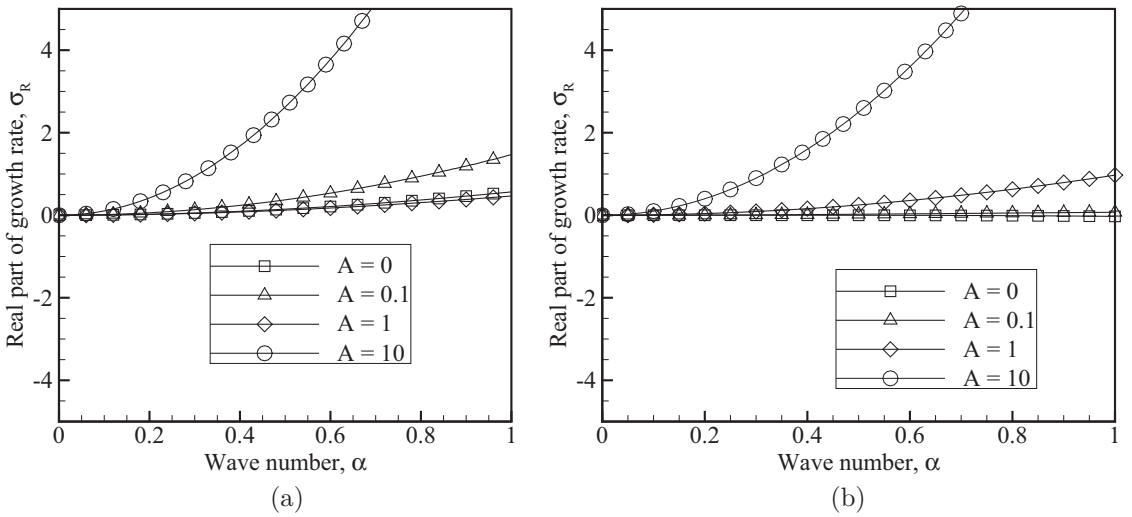

FIG. 5. Growth rate variation with the wave number for different values of dimensionless disjoining pressure A with $N_D = 0.1$, $S = 0.1$, $Z_R = 0$ and (a) $N_{EO}/E_R = 2500$, (b) $N_{EO}E_R = 0.01$.

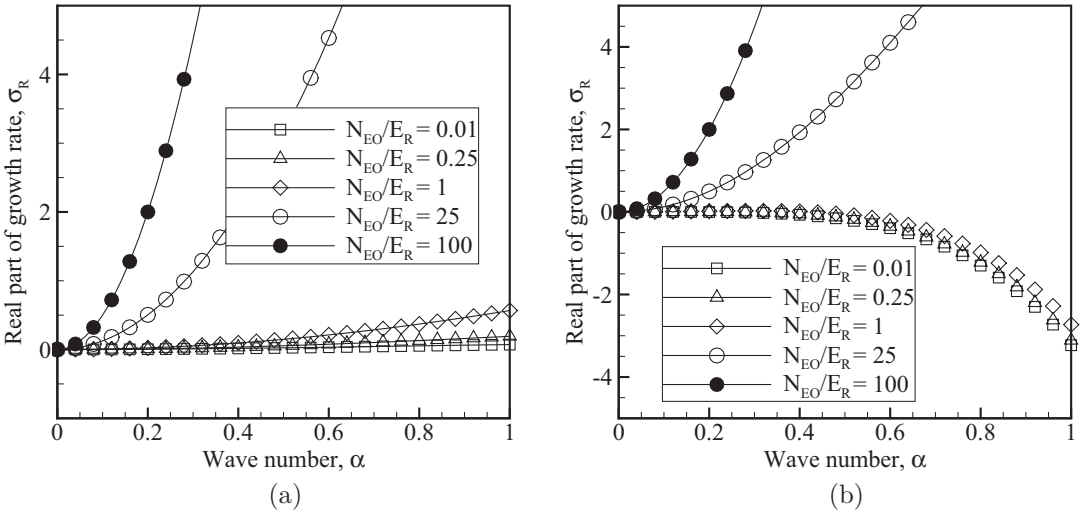

FIG. 6. Growth rate variation with the wave number for different values of the applied electric field with $A = 0.1$, $N_D = 0.1$, $Z_R = 0$ and (a) $S = 0.1$, (b) $S = 10$.

from the mechanical equilibrium of the thin film hence making the system unstable.

The effect of the externally applied electric field, which can be reflected through the ratio, $\frac{N_{EO}}{E_R}$ on the stability of the system is clearly observed from Eq. (37), which shows that the increase of the applied electric field makes the system more unstable. This is an expected phenomenon, as upon increasing the magnitude of the electric field E_{ext} the unbalanced interfacial stress components due to the resulting Maxwell stress increase, pushing the system away from equilibrium. This effect is shown in Fig. 6 for two values of S.

It is also known that, influenced by the nature of the substrate-fluid interactions and the fluid properties, the interfacial zeta potential is determined and can be measured experimentally. Under electro-osmotic flows, the effect of the substrate zeta potential ζ_b has a significant effect on the interfacial stability of thin films. This is shown in Fig. 7 for two characteristic values of $N_{EO}E_R, N_D, S$ and fixed value of A. As can be seen from the expression of the growth factor [Eqs. (35) through (37)], the product $N_{EO}E_R$, which is proportional to ζ_b^2, has a negative coefficient and leads to a decrease in the growth factor when the substrate zeta potential is increased. Hence, when the substrate zeta potential is increased, the system becomes more stable, which is clearly shown in Fig. 7.

From the basic state velocity distribution [see Eq. (29)], one can see that depending upon the interfacial zeta potential the interface can either reduce the interfacial stress or enhance it. This is also shown in Fig. 8 where one can also see that when the interface has an opposite polarity as compared to the substrate, it reduces the interfacial stress and when the free surface polarity is the same as the substrate, it supports the interfacial stress. This relation between interfacial polarity and interfacial stress also manifests itself in the system stability equations [Eqs. (35) through (37)] as expected. It is observed that the interfacial polarity with respect to the substrate zeta

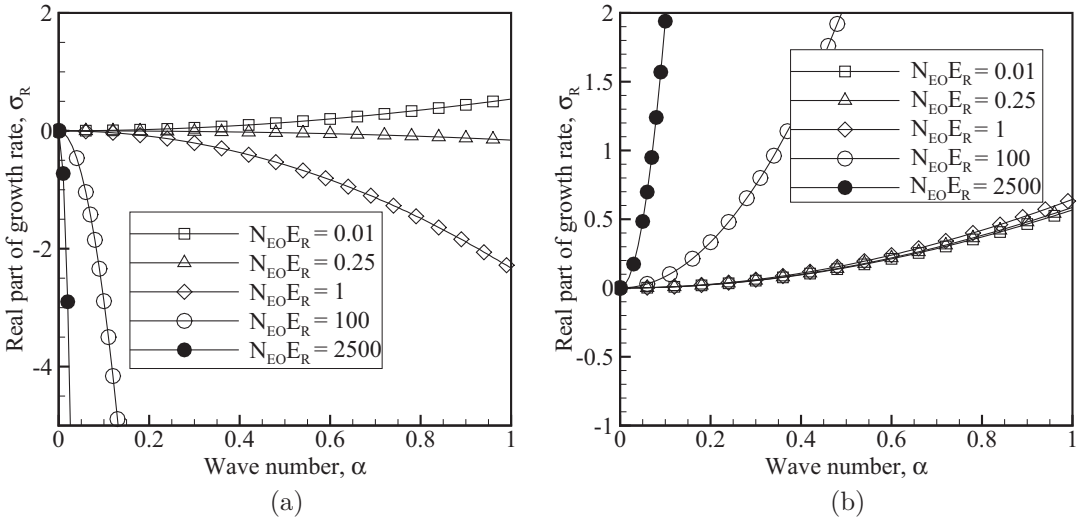

FIG. 7. Growth rate variation with the wave number for different values of substrate zeta potential with $N_D = 0.5$, $S = 0.1$, $A = 0.1$ and (a) $Z_R = -1$, (b) $Z_R = 1$.

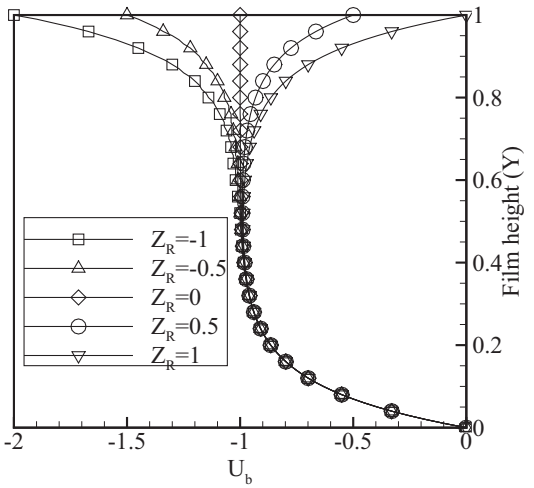

FIG. 8. The base state velocity profile with different values of the surface to substrate potential ratio (Z_R). The values of other fixed parameters are $N_{EO} = 1$, $N_D = 0.1$.

potential, which is represented by the ratio Z_R, tends to increase the system stability as it reduces the interfacial stress when Z_R is negative (i.e., of the opposite polarity to the substrate). The system becomes more unstable when Z_R is positive (i.e., of the same polarity as of the substrate as it enhances the interfacial stress). This effect is shown in Fig. 9. This can also be attributed to the impact of the substrate zeta potential on the distribution of charged species in the bulk of the fluid. As the zeta potential increases, the concentration of counterion species increases near the substrate, decreasing the ionic concentration in the bulk which screens the magnitude of the net electric potential as felt at the interface. This decreases the contributions of the charged substrate to the interfacial Maxwell stress hence making the system more stable. This mechanism is also clearly highlighted in Fig. 7, which shows the growth rate variation for two opposite values of Z_R with $N_{EO}E_R$ as the varying parameter and all the other parameters being fixed.

The effect of the initial film thickness as compared to the Debye length, represented by Debye number N_D, on the interfacial stability is not obvious by observing the

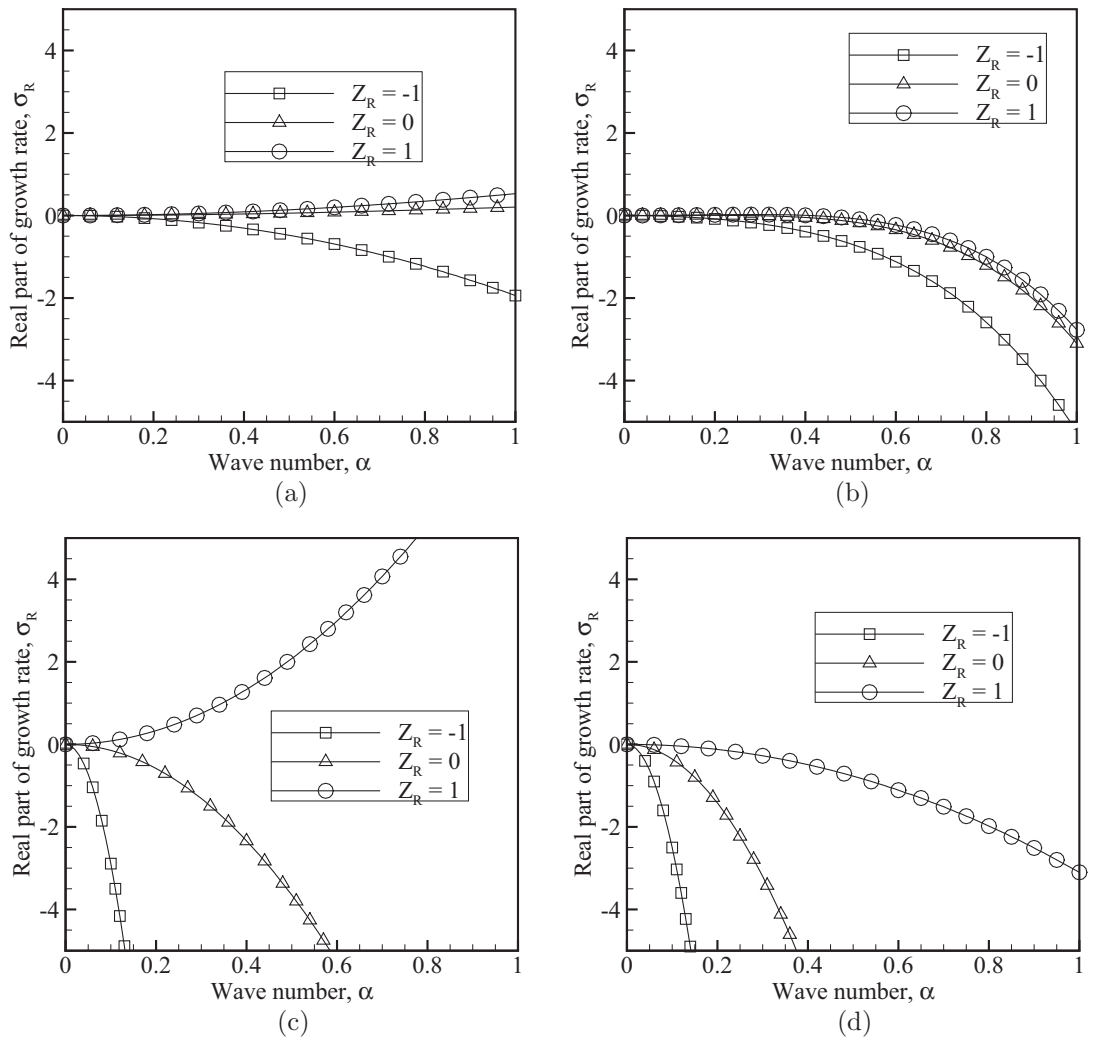

FIG. 9. Growth rate variation with the wave number for different values of the interfacial zeta potential. The values of other fixed parameters are (a) $N_{EO}E_R = 1$, $N_D = 1$, $S = 0.1$, $A = 0.1$, (b) $N_{EO}E_R = 1$, $N_D = 1$, $S = 10$, $A = 0.1$, (c) $N_{EO}/E_R = 100$, $N_D = 0.5$, $S = 0.1$, $A = 0.1$, (d) $N_{EO}/E_R = 100$, $N_D = 1$, $S = 0.1$, $A = 0.1$.

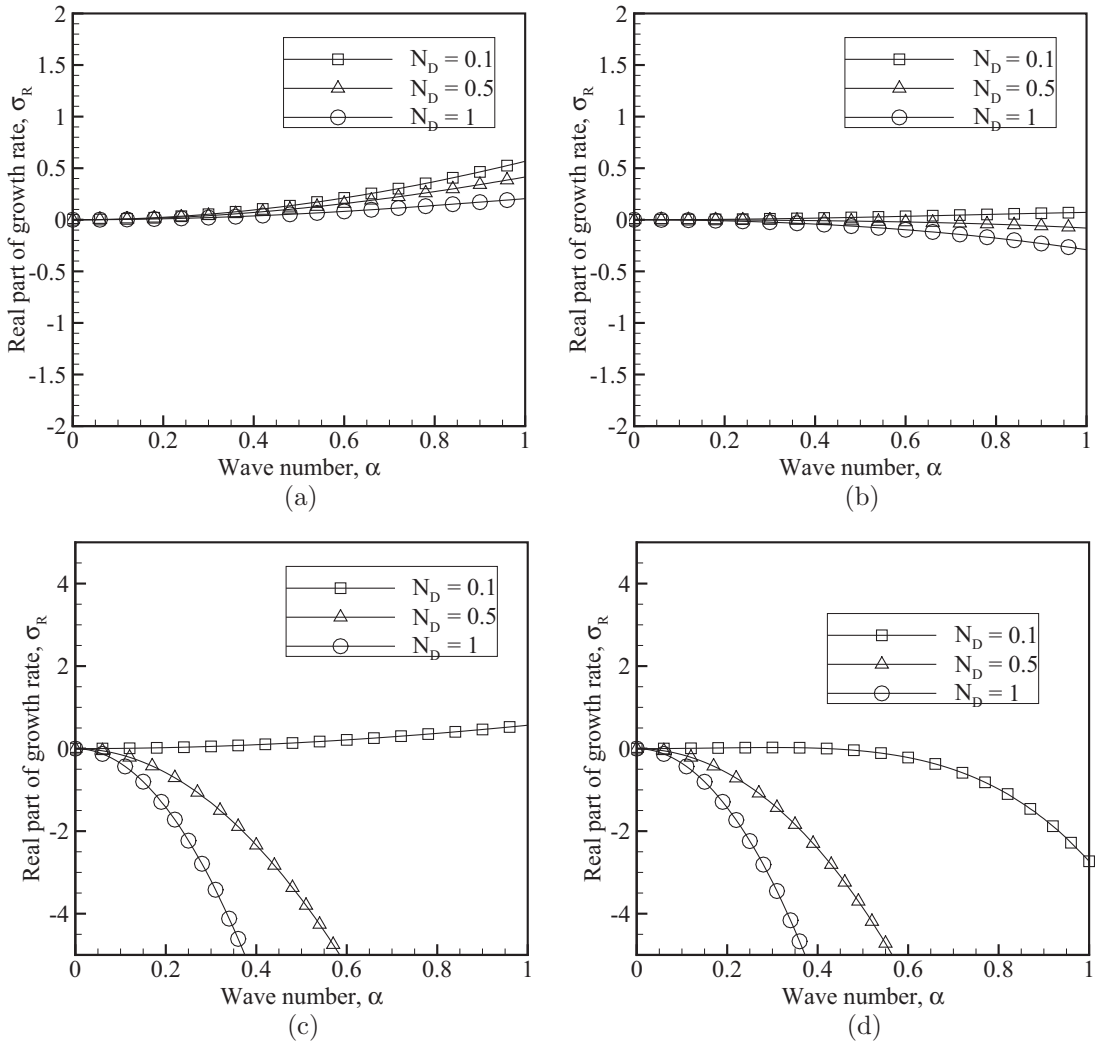

FIG. 10. Growth rate variation with the wave number for different values of the Debye number, which corresponds to a varying Debye length for a given film thickness. The values of other fixed parameters are (a) $N_{EO}E_R = 1$, $Z_R = 0$, $S = 0.1$, $A = 0.1$, (b) $N_{EO}E_R = 0.01$, $Z_R = 0$, $S = 0.1$, $A = 0.1$, (c) $N_{EO}/E_R = 100$, $Z_R = 0$, $S = 0.1$, $A = 0.1$, (d) $N_{EO}/E_R = 100$, $Z_R = 0$, $S = 10$, $A = 0.1$.

growth factor characteristic equation [Eqs. (35) through (37)]. Figure 10 shows the effect of N_D on the stability of the system for different values of all the other parameters. It is observed from this figure that the stability of the system increases upon increasing N_D. This can be explained by the fact that for a given film thickness d, an increase in Debye number corresponds to an increasing Debye length, which in turn corresponds to a decrease in ionic concentration as $\lambda_D \propto \frac{1}{\sqrt{c_0}}$, where c_0 is the ionic concentration. Hence, a decrease in the ionic concentration drives the system naturally toward stability. The flow actuating mechanism in this problem is the Coulombic force acting in the fluid by the external electric field to the distribution of ions in the fluid. If the ionic concentration c_0 is low, so will be the net forces by the external electric field on the ionic solution. Hence, in this limit of large N_D, the flow will be reduced and consequently the interface will stay undisturbed.

Conditions leading to the onset of instability can be complemented by a study of a mode that corresponds to the maximum growth rate of a disturbance. This mode, which is characterized as the most dangerous mode (α_{critical}), is studied as a function of the set of parameters mentioned above. The most dangerous mode is the wave number for which the characteristic stability curve [Eq. (35)] of a system reaches a maximum. The resulting wave number is obtained as a function of dimensionless parameters through the following equation:

$$\alpha_{\text{critical}} = \sqrt{\frac{-g(A, N_{EO}, E_R, Z_R, N_D)}{2f(S)}}, \tag{38}$$

with a condition that $g(A, N_{EO}, E_R, Z_R, N_D)$ is positive.

The α_{critical} as obtained from the above equation was studied for the various dimensionless parameters and representative results are presented in Figs. 11 to 13. The increase in van der Waals parameter (A) increases the value of α_{critical} (see Fig. 11). It is also observed that the increase in the value of surface tension decreases the value of α_{critical}, which is

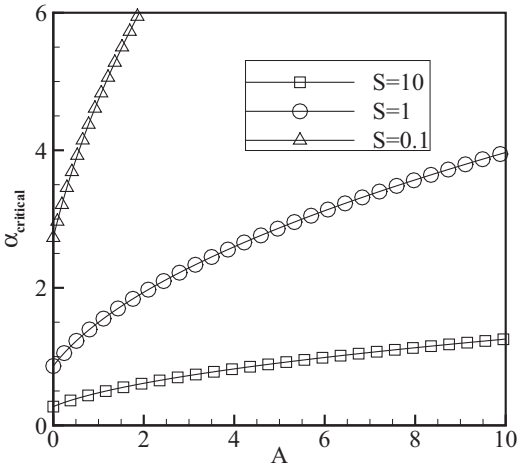

FIG. 11. Most dangerous wave number (α_{critical}) variation with the van der Waals parameter (A), for different values of the surface tension parameter (S). Values of other fixed parameters are $N_{EO}E_R = 1$, $N_D = 1$, $Z_R = 0$.

consistent with the observation that an increase in surface tension increases the stability of the system by decreasing the most dangerous mode. It is observed that the most dangerous mode is independent of Debye number for $\lambda_D > d/2$ (see Fig. 12) and suggests that the most dangerous wavelength is of the order of the film thickness in this range of N_D, independently of the other parameters. For a given value of the Debye number, α_{critical} increases with the wall zeta potential ($N_{EO}E_R$) (see Fig. 12). Finally, the most dangerous mode is independent of the polarity of the interface zeta potential (Z_R) and increases with its magnitude (see Fig. 13). Also, the increase in the magnitude of the external electric field (N_{EO}/E_R) increases the value of the most dangerous mode.

VI. CONCLUSION

In this work, the stability of the free surface of an ultrathin liquid film under electro-osmotic flow conditions

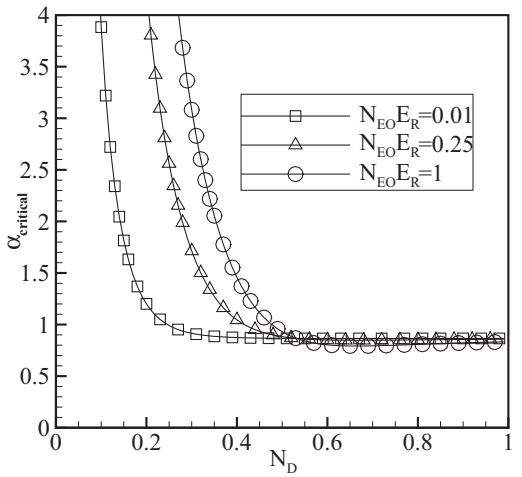

FIG. 12. Most dangerous wave number (α_{critical}) variation with the Debye number (N_D) for different values of the wall zeta potential ($N_{EO}E_R$). Values of other fixed parameters are $S = 1$, $Z_R = 1$, $A = 0$.

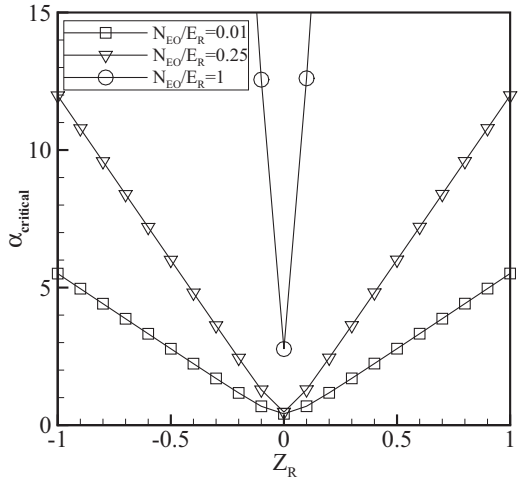

FIG. 13. Most dangerous wave number (α_{critical}) variation with the zeta potential ratio (Z_R) for different values of the electric field parameter (N_{EO}/E_R). Values of other fixed parameters are $S = 10$, $N_D = 0.1$, $A = 1$.

was investigated. Through long-wave asymptotic analysis of the Orr-Sommerfeld equations, a complex dependence of the film stability on various parameters like surface tension, Hamaker's constant for fluid-substrate interaction, magnitude of the externally applied electric field, substrate, and free surface zeta potential was highlighted. It was observed that ignoring the free surface Maxwell stress under electro-osmotic flow, overestimates the free surface instability. The presented characteristic stability curve helps to identify the critical values of various parameters presented in the paper, which can be effective in designing thin film flow process in microfluidic devices. Some of the parameter-dependent stability trends are summarized as follows.

(a) The surface tension increases the interfacial stability as expected and has a stabilizing effect for small wavelength disturbances.

(b) It is observed that the film stability decreases upon increasing the magnitude of the applied electric field: this is due to an increase in the Maxwell stresses at the interface.

(c) The increase in the value of substrate zeta potential tends to stabilize the flow.

(d) The interfacial zeta potential has a rather interesting effect on the thin film stability. In general, it is seen that upon increasing the magnitude of the interfacial zeta potential, the film stability decreases and at the same time, if the interfacial zeta potential is of the opposite polarity of the substrate, it increases the film stability.

(e) It is also observed that increasing the magnitude of the disjoining pressure reduces film stability.

(f) Finally, it was also shown that the increase in Debye length, which corresponds to an increase in Debye number (i.e., to a decrease of the ionic concentration for a given film thickness) increases film stability.

APPENDIX

The solution of the Orr-Sommerfeld equations [Eq. (32)] is obtained using the asymptotic expansion [Eq. (33)] method.

The set of equations with α^0 order are as follows

$$D^4\Psi_0 = 0, \tag{A1}$$

with the boundary conditions as

$$\Psi_0(0) = 0, \quad D\Psi_0(0) = 0, \quad D^2[\Psi_0(1) + \eta U_b(1)] = 0, \quad D^3\Psi_0(1) = 0, \quad \Psi_0(1) - \eta[C_0 - U_b(1)] = 0. \tag{A2}$$

Upon solving the above set of equations the solution in Ψ_0 is

$$\Psi_0(Y) = -\frac{N_{EO}Y^2Z_R\eta}{2{N_D}^2} \tag{A3}$$

and the C_0 can be obtained as

$$C_0 = N_{EO}\left\{-1 + Z_R\left(1 - \frac{1}{2{N_D}^2}\right)\right\}. \tag{A4}$$

The set of equations with α^1 order are as follows:

$$D^4\Psi_1 = -\{[C_0 - U_b(Y)]D^2\Psi_0(Y) + D^2U_b(Y)\Psi_0(Y)\} \tag{A5}$$

with the boundary conditions as

$$\begin{aligned}
\Psi_1(0) &= 0,\\
D\Psi_1(0) &= 0,\\
D^3\Psi_1(1) + [C_0 - U_b(1)]\,D\Psi_0(1) + DU_b(1)\Psi_0(1) + \eta(3A - \alpha^2 S) &= 0,\\
D^2\Psi_1(1) - \eta N_{EO}E_R\left((\partial_X\Phi)^2 - (\partial_Y\Phi)^2\right) &= 0.
\end{aligned} \tag{A6}$$

Upon solving Eq. (A5), with the boundary conditions Eqs. (A6), the solution of $\Psi_1(Y)$ is

$$\begin{aligned}
\Psi_1(Y) = &-\frac{1}{2}AY\eta + \frac{3}{2}AY^3\eta + \frac{N_{EO}Y^3\eta}{2E_R} - 9N_D^2N_{EO}^2Z_R\eta - N_{EO}^2Y^3Z_R^2\eta + \frac{N_{EO}^2Y^3Z_R^2\eta}{8N_D^4} - \frac{N_{EO}^2Y^3Z_R^2\eta}{2N_D^2}\\
&-\frac{N_{EO}E_RY^3Z_R^2\eta}{2N_D^2} - \frac{N_{EO}^2Y^4Z_R^2\eta}{48N_D^4} + \frac{N_{EO}^2Y^4Z_R^2\eta}{24N_D^2} + \frac{1}{6}SY\alpha^2\eta - \frac{1}{2}SY^3\alpha^2\eta + 9N_D^2N_{EO}^2Z_R\mathrm{Cosh}\left(\frac{Y}{N_D}\right)\eta\\
&+\frac{1}{2}N_{EO}^2Y^2Z_R\mathrm{Cosh}\left(\frac{Y}{N_D}\right)\eta + 4N_DN_{EO}^2YZ_R\mathrm{Cosh}\left(\frac{Y}{N_D}\right)\mathrm{Coth}\left(\frac{1}{N_D}\right)\eta - \frac{N_{EO}^2Y^3Z_R\mathrm{Cosech}\left(\frac{1}{N_D}\right)\eta}{N_D}\\
&-5N_DN_{EO}^2Y^2Z_R^2\mathrm{Cosech}\left(\frac{1}{N_D}\right)\eta - 4N_DN_{EO}^2YZ_R^2\mathrm{Cosh}\left(\frac{Y}{N_d}\right)\mathrm{Cosech}\left(\frac{1}{N_D}\right)\eta\\
&+\frac{N_{EO}E_RY^3Z_R\mathrm{Coth}\left(\frac{1}{N_D}\right)\mathrm{Cosech}\left(\frac{1}{N_D}\right)\eta}{N_D^2} - \frac{N_{EO}E_RY^3\mathrm{Cosech}\left(\frac{1}{N_D}\right)^2\eta}{2N_D^2} - \frac{N_{EO}E_RY^3Z_R^2\mathrm{Cosech}\left(\frac{1}{N_D}\right)^2\eta}{2N_D^2}\\
&+\frac{5}{2}N_DN_{EO}^2Y^2Z_R\mathrm{Cosech}\left(\frac{1}{N_D}\right)^2\mathrm{Sinh}\left(\frac{2}{N_D}\right)\eta + \frac{N_{EO}^2Y^3Z_R^2\mathrm{Cosech}\left(\frac{1}{N_D}\right)^2\mathrm{Sinh}\left(\frac{2}{N_D}\right)\eta}{2N_D}\\
&-4N_DN_{EO}^2YZ_R\mathrm{Sinh}\left(\frac{Y}{N_D}\right)\eta - 9N_D^2N_{EO}^2Z_R\mathrm{Coth}\left(\frac{1}{N_D}\right)\mathrm{Sinh}\left(\frac{Y}{N_D}\right)\eta - \frac{1}{2}N_{EO}^2Y^2Z_R\mathrm{Coth}\left(\frac{1}{N_D}\right)\mathrm{Sinh}\left(\frac{Y}{N_D}\right)\eta\\
&+9N_D^2N_{EO}^2Z_R^2\mathrm{Cosech}\left(\frac{1}{N_D}\right)\mathrm{Sinh}\left(\frac{Y}{N_D}\right)\eta + \frac{1}{2}N_{EO}^2Y^2Z_R^2\mathrm{Cosech}\left(\frac{1}{N_D}\right)\mathrm{Sinh}\left(\frac{Y}{N_D}\right)\eta.
\end{aligned} \tag{A7}$$

C_1 can be obtained from the kinematic boundary condition as

$$C_1 = \frac{\Psi_1(1)}{\eta}. \tag{A8}$$

[1] H. Lin, Mech. Research Comm. **36**, 33 (2009).

[2] B. Zaltzman and I. Rubinstein, J. Fluid Mech. **579**, 173 (2007).

[3] I. Rubinstein, B. Zaltzman, and I. Lerman, Phys. Rev. E **72**, 011505 (2005).

[4] B. Y. Rubinstein and A. M. Leshansky, Phys. Rev. E **83**, 031603 (2011).

[5] T. L. Sounart and J. C. Baygents, J. Fluid Mech. **576** 139 (2007).

[6] J. J. Santos and B. D. Storey, Phys. Rev. E **78**, 046316 (2008).

[7] M. H. Oddy, J. G. Santiago, and J. C. Mikkelsen, Anal. Chem. **73**, 5822 (2001).
[8] C. H. Chen, H. Lin, S. K. Lele, and J. G. Santiago, J. Fluid Mech. **524**, 263 (2005).
[9] J. Posner and J. G. Santiago, J. Fluid Mech. **555**, 1 (2006).
[10] M. H. Oddy and J. G. Santiago, Phys. Fluids **17**, 064108 (2005).
[11] M. Smoluchowsky, Krak. Anz. **8**, 182 (1903).
[12] H. Kim, S. G. Bankoff, and M. J. Miksis, Phys. Fluids A **4**, 2117 (1992).
[13] S. Qian, S. W. Joo, Y. Jiang, and M. A. Cheney, Mech. Research Comm. **36**, 82 (2009).
[14] I. M. R. Sadiq and S. W. Joo, Microgravity Sci. Tech. **21**, S331 (2009).
[15] S. W. Joo, J. Mech Sci. Tech. **22**, 382 (2008).
[16] W. Choi, A. Sharma, S. Qian, G. Lim, and S. W. Joo, J. Coll. Inter. Sci. **347**, 153 (2010).
[17] C. S. Yih, Phys. Fluids **6**, 321 (1963).
[18] A. Oron, S. H. Davis, and S. G. Bankoff, Rev. Mod. Phys. **69**, 931 (1997).
[19] V. Padmanabhan, J. Daillant, L. Belloni, S. Mora, M. Alba, and O. Konovalov, Phys. Rev. Lett. **99**, 086105 (2007).
[20] G. Y. Tang, C. Yang, J. C. Chai *et al*., Int. J. Heat Mass Transf. **47**, 215 (2004).
[21] B. J. Kirby and E. F. Hasselbrink, Electrophoresis **25**, 187 (2004).
[22] B. V. Derjaguin and N. V. Churaev, J. Coll. Inter. Sci. **66**, 389 (1978).
[23] S. V. Alekseenko, V. E. Nakoryakov, B. G. Pokusev, *Wave Flow in Liquid Flims* (Begell House, New York, 1994).